Origin of Moiré structures in C_{60} on Pb(111) and their effect on molecular energy levels

H. I. Li,[1] K. J. Franke,[2] J. I. Pascual,[2] L. W. Bruch,[3] and R. D. Diehl[1]

[1]*Department of Physics, Penn State University, University Park, Pennsylvania 16802, USA*
[2]*Institut für Experimentalphysik, Freie Universität Berlin, Arnimalee 14, 14195 Berlin, Germany*
[3]*Department of Physics, University of Wisconsin, Madison, Wisconsin 53706, USA*

Low-energy electron diffraction (LEED) indicates that the monolayer structure of C_{60} on Pb(111) comprises two coexisting incommensurate structures with nonsymmetry epitaxial rotations near 20° relative to the Pb(111) lattice. These structures are observed in scanning tunneling microscopy (STM) as Moiré superstructures having periods of about 46 Å and 34 Å. The Moiré images and LEED patterns are consistent with two higher-order commensurate (HOC) structures that were identified using the hexagonal number sequence method. These structures are close to predictions from the Novaco-McTague theory of epitaxial rotation, assuming a weakly corrugated substrate potential. As a consequence of the fullerenes within the Moiré structures having different local environments, the energetic alignment of the molecular resonances is also modulated, with shifts measured by tunneling spectroscopy of up to 20 meV.

I. INTRODUCTION

Fullerene-based molecular crystals and films have been of interest for some time because of their very rich electronic properties, including superconductivity with high critical temperatures, ferromagnetism and metal-insulator transitions.[1] The interfaces of C_{60} films with metal surfaces are of particular interest for molecular electronics applications.[2] Fullerene films are also of interest from a fundamental perspective, because they represent a class of relatively simple model structures for studying the interactions of gases with carbon materials.[3] On close-packed metal surfaces, commensurate structures are often formed, for instance a $(2\sqrt{3} \times 2\sqrt{3})R30°$ structure on Ag(111)[4–9] or Au(111),[4,8,10–12] a (4×4) structure on Cu(111)[6,7,11,13,14] and a $(\sqrt{13} \times \sqrt{13})R13.9°$ structure on Pt(111).[15] Many of these structures are accompanied by a substrate reconstruction, evidence of a strong C_{60}-metal interaction.[16] However, the C_{60}-C_{60} interaction also is an important factor in the structures of these films. The fact that the C_{60}-C_{60} distance is usually close to its natural spacing of about 1 nm, along with the fact that in some of these cases there are structures that are not simply commensurate, indicates that the strength of the C_{60}-C_{60} van der Waals attraction is comparable to the magnitude of the lateral energy variation in the C_{60}-substrate interaction.[17]

A monolayer of C_{60} on Pb(111) forms a structure that is close-packed, with an average lattice spacing that is not a simple superlattice of Pb(111), and is rotated relative to the Pb(111) lattice. Nonsymmetry rotations for incommensurate monolayers have been studied for many years and can be interpreted in several ways. The Novaco-McTague (NM) epitaxial rotation theory treats the relaxation of an elastic overlayer in response to an incommensurate substrate potential,[18,19] the rotation angle depending on the mismatch between the overlayer and substrate lattices. The exact rotational behavior depends on the overlayer-overlayer and overlayer-substrate interactions.[20–22] Where the corrugation

is higher, however, a description based on domain wall alignment[23] becomes useful. Discrete structures can be identified using a higher-order commensurate (HOC) structure analysis, which is more applicable if the average domain size is limited.[24] In that case, instead of a continuous variation in average rotation angle, the angle may change discretely as a function of lattice mismatch, as the overlayer adopts one HOC after the other, behavior known as a "devil's staircase."[25]

In incommensurate or higher-order commensurate films, the competition of the substrate and overlayer lattice periodicities produces a Moiré pattern that is evident as height variations in scanning tunneling microscopy (STM) or as additional peaks in the diffraction pattern. The Moiré pattern has a period much larger than the overlayer lattice spacing, and the adsorbate molecules occupy a variety of adsorption sites. The Moiré unit cell may correspond to a HOC structure, with a repeat distance equal to or larger than the Moiré period. A systematic procedure for predicting, identifying and classifying HOC structures was recently proposed[24] and has been applied here. The observed structures were also compared to calculations based on the Novaco-McTague (NM) theory. As a consequence of the C_{60} molecules having different local environments, the energetic alignment of the molecular resonances is also modulated. This modulation was measured with tunneling spectroscopy, as described below.

II. EXPERIMENT

A. Procedures

The low-energy electron diffraction (LEED) experiments were carried out at Penn State and the STM experiments were carried out at the Freie Universität Berlin. The procedures for preparing the Pb(111)[26] and the C_{60} films were similar, consisting of ion bombardment and annealing to 160–200 °C, followed by dosing the C_{60} onto a room tem-
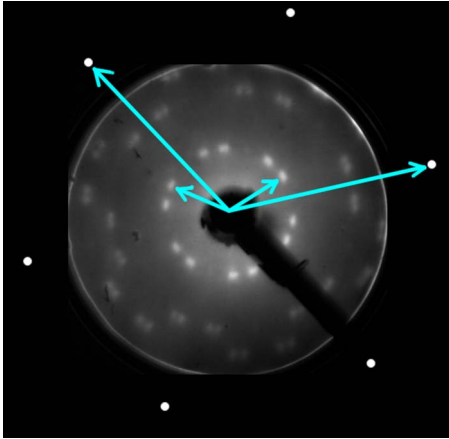
FIG. 1. (Color online) LEED pattern for one monolayer of C_{60} on Pb(111) using an incident beam energy E=34 eV. The locations of the first-order Pb spots are indicated outside the actual LEED pattern. The reciprocal lattice vectors for the Pb (long arrows) and reciprocal lattice vectors showing the average C_{60} lattice (short arrows) are shown. The C_{60} spots are split, but the splitting is resolved only for the higher-order diffraction peaks. The pattern as shown does not scale linearly in momentum space due to the flat-plate geometry.

perature crystal. The film was annealed to at least 120 °C and then cooled to 77 K for LEED measurements and 5 K for STM measurements.

The LEED instrument used in these studies was an OCI™ low-current LEED system. The data were acquired using a video data acquisition system to acquire whole LEED pattern frames. The LEED patterns presented here are not corrected for the distortion that occurs when imaging onto the flat-plate detector. However, the flat-plate correction was applied to the measurements taken from the LEED patterns. While the locations of the LEED spots did not change in the submonolayer regime, the overlayer spots grew in intensity and clarity as the coverage increased. The highest-intensity pattern was taken to be a coverage of one monolayer. The STM was a low-temperature instrument that was home-built at Freie Universität Berlin.

B. Results

Figure 1 shows the LEED pattern from a monolayer of C_{60} on Pb(111) at an electron beam energy of 34 eV and a sample temperature of 80 K, where the nearest-neighbor spacing of the Pb atoms is 3.48 Å. The six first-order substrate spots are not visible on the screen at this energy; their locations are indicated with white circles. The three additional rings of spots are due to the C_{60} overlayer. In the outer two rings, twelve split spots per ring are evident, giving 24 individual spots per ring. The splitting is not resolved in the inner ring, but those spots are azimuthally elongated. The ratios of the diameters of the rings is $1:\sqrt{3}:2$, indicating that the overlayer structure is hexagonal, and the 24 spots per ring indicates that there are four rotational domains. The
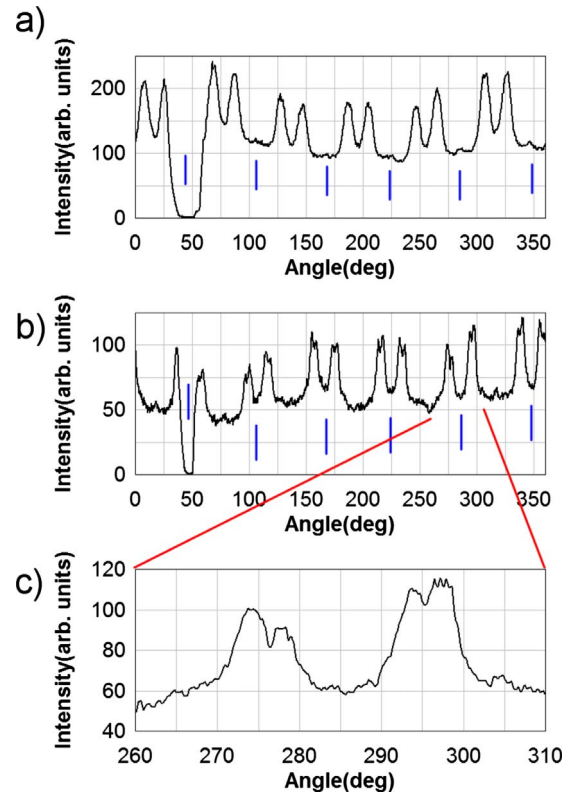

FIG. 2. (Color online) (a) Intensity profile around the inner ring of diffraction spots (corresponding to 10 Å nearest-neighbor distance) evident in Fig. 1. The profiles correspond to a clockwise traversal. (b) Intensity profile around the outer ring, where the spot splitting is resolved. The vertical (blue) bars indicate the angles of the Pb spots. (c) Magnification of a section of (b).

average C_{60}-C_{60} distance was determined by measuring the ratio of the inner overlayer spot radial positions to those of the Pb spots, $R=0.348\pm0.004$, giving an average C_{60}-C_{60} nearest-neighbor distance of 10.0 ± 0.1 Å. Angular profiles of the diffraction rings are shown in Fig. 2. The rotated spots are symmetric around the substrate beams, indicating the presence of four equivalent domains rotated $\pm18.6°\pm0.7°$ and $\pm22.4°\pm0.7°$ relative to the substrate symmetry directions. The intensities of all spots are similar, suggesting equal or nearly equal occupation of each type of domain. No difference was found between LEED patterns obtained after postdeposition anneals between 100 °C and 200 °C, and the pattern was the same for various submonolayer coverages.

Figure 3 shows two representative STM images from the C_{60} monolayer on Pb(111). In agreement with the LEED analysis, the C_{60} molecules form a hexagonal lattice with a period of about 10 Å. Additionally, there is a faint longer-range modulation of the height of the molecules, indicating two different Moiré structures having periods of about 34 and 46 Å. In the smaller superstructure, the C_{60} rows are aligned with the Moiré lattice, whereas in the larger one, the Moiré lattice is rotated by about 11° relative to the C_{60} lattice.

A consequence of the large superstructures is that the C_{60} molecules are located in several slightly different environments with respect to the substrate. Schull and Berndt re-
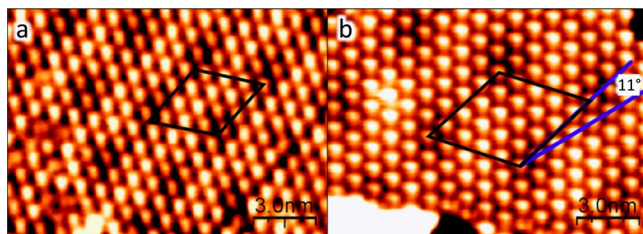
FIG. 3. (Color online) Constant current STM images of C$_{60}$ on Pb(111) for (a) the 34 Å Moiré structure and (b) the 46 Å Moiré structure. The fullerenes are in a close-packed structure. The Moiré superstructures appear as faint hexagonal height modulations in the STM images. The unit cells of the Moiré structures are indicated by rhombuses. The (a) 34 Å Moiré is aligned with the C$_{60}$ lattice, whereas the (b) 46 Å Moiré is rotated 11° with respect to the C$_{60}$ lattice.

cently showed that for C$_{60}$ on Au(111), long-range superstructures result in gradual changes in the orientation of the fullerene cage with respect to the substrate.[17] However, on Pb(111) we do not observe this effect, as can be inferred from Fig. 4. Most of the molecules are imaged as round protrusions in STM images at positive sample bias (i.e., tunneling into unoccupied molecular states). Only a minority of molecules shows a distinct intramolecular resolution, with features having a characteristic threefold or twofold symmetry. It has been shown previously[12] that such structures correspond to the shape of the lowest unoccupied molecular orbital (LUMO). Thus, they indicate that the molecules lie with their C3 or C2 axes oriented perpendicular to the surface. The occurrence of these orientations is very rare in the observed STM images and do not account for the Moiré superstructure.

Although the local adsorption environment does not visibly influence the molecular orientation, we have found an effect on the electronic structure of the molecular layer. While constant current STM images, as shown in Fig. 3, resolve small modulations in the apparent height of the molecules on the substrate, differential conductance maps are better suited to disentangle geometric and electronic contributions. Hence, we have simultaneously recorded topographic and differential conductance maps, as shown in Figs. 5(a) and 5(b). Their comparison shows that the Moiré structure is even more evident in the differential conductance maps.
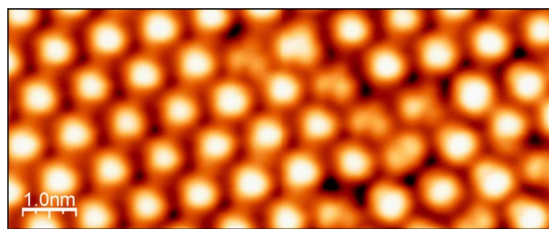

FIG. 4. (Color online) High resolution STM image resolving the orientation of the fullerene cages. The majority of molecules appear as round protrusions indicating a similar orientation and/or adsorption state, while a minority with threefold (C3) and twofold (C2) orientation are also apparent.
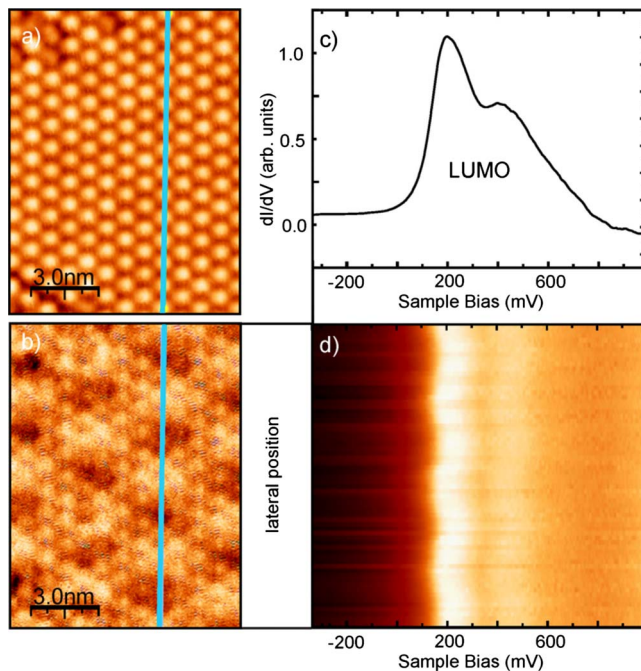

FIG. 5. (Color online) (a) STM image of the 34 Å superstructure and (b) its differential conductance map at 0.3 V. (c) Differential conductance spectrum reflecting the LUMO derived resonance of one fullerene. (d) Differential conductance profile along the vertical (blue) line marked in (b) of C$_{60}$ molecules across the Moire structure. The LUMO shifts by 20 meV with the periodicity of the superstructure, while the overall line shape is preserved.

In order to track its origin, we have analyzed the alignment of the LUMO with respect to the Pb Fermi level along a molecular row across the Moiré modulation. The LUMO derived resonance is observed as a peak with a characteristic split structure [Fig. 5(c)], which we tentatively assign to the lifting of the threefold degeneracy upon adsorption on the Pb(111) surface.[17,27] Figure 5(d) shows a map of this peak (dI/dV in a color scale) as a function of the position along the line shown in Fig. 5(a). As can be seen, the peak height and line shape remains unaffected in all the spectra taken along the line, thus ruling out that the Moiré modulation appears from local changes in the chemical state of the fullerenes or from their orientation.[28,29] Instead, the dI/dV map shows that the peak alignment undergoes shifts of about 20 mV in phase with the observed Moiré structure in Fig. 5(b). The origin of this energy shift can be related to variations in the local screening properties of each fullerene, depending on their position in the HOC structure. In particular, the darker position of the dI/dV map can be related to sites in which the LUMO appears at higher energy values with respect to the Fermi energy. According to a simple model of screening of local charges in molecules by metal surfaces,[30] the LUMO peak is expected to appear at higher energy positions in molecules lying higher from the surface.[31] In this case, the higher LUMO alignment could be simply associated to molecules on top sites, which may be higher than, for example, molecules on hollow sites.

TABLE I. Thermodynamic parameters for monolayer triangular lattices of C_{60} with the G and PR models carried to the fourth shell of neighbors. E/N is the potential energy per molecule, Φ is the 2D spreading pressure, and $B = -Ad\Phi/dA$ is the bulk modulus. Assuming that Pb $L_{nn} = 3.48$ Å, $L = 10.45$ is a misfit of $+0.1\%$ relative to the 3×3 commensurate lattice ($=10.44$ Å) and $L = 9.3$ is $+1\%$ relative to the $(\sqrt{7} \times \sqrt{7})R19.1°$ lattice ($=9.21$ Å). L_{nn} for the unconstrained monolayer is $L_u = 10.052$ Å for the G model and 10.013 Å for the P-R model. Conversion to SI: 1 meV $=1.6 \times 10^{-22}$ J, 1 meV A$^{-2} = 0.016$ J m^{-2}.

L_{nn} (Å)	Girifalco			Pacheco-Ramalho		
	E/N (meV)	Φ (meV A^{-2})	B (meV A^{-2})	E/N (meV)	Φ (meV A^{-2})	B (meV A^{-2})
10.45	−719	−26.1	24.6	−696	−23.8	59.8
L_u	−850	0	896	−819	0	591
9.95	−831	24.1	1520	−814	8.27	730
9.90	−803	41.5	1960	−804	16.3	857
9.85	−758	64.1	2510	−786	25.7	1000
9.8	−692	93.1	3210	−760	36.7	1160
9.75	−598	130	4100	−723	49.5	1340
9.70	−469	178	5240	−675	64.4	1540
9.4	1827	939	23400	−38.0	213	3370
9.3	3835	1594	39500	370	295	4300

III. MODELING AND ANALYSIS

A. General considerations

A weakly bound C_{60} monolayer has many similarities to prototypical physical adsorption systems, e.g., rare gases and small molecules, but the energy scales are much larger. The shape of the intermolecular potential is also different. While the van der Waals interaction still provides the primary attraction between adsorbed C_{60} molecules, the short range C_{60}-C_{60} repulsion is much steeper, narrowing the range of monolayer compression. Also, the C_{60} length scale is much longer than the substrate length scale.

The three-dimensional (3D) solid C_{60} has an fcc lattice at 300 K with a nearest-neighbor spacing of $L_{nn} = 10.02$ Å. A transition to an orientationally ordered solid with an sc lattice and $L_{nn} = 9.93$ Å occurs at about 250 K.[32] The bulk modulus of the fcc solid is 1.4×10^{10} Pa (Ref. 33) and the heat of sublimation is 1.74 eV/molecule.[34] In modeling the fcc solid, the atomic discreteness of the C_{60} becomes significant (about 20% of the pressure) at $L_{nn} = 9.76$ Å.[35]

In most physical adsorption systems studied to date, the ratio of the substrate bulk modulus to that of the bulk adsorbate solid is so large that measurable deformations are limited to the adlayer. For instance, the ratio is 75 for Pt relative to Xe, and 27 for Ag relative to Xe.[36,37] It is only 3 for Pb relative to C_{60}, reflecting both the softness of Pb and the stiffness of C_{60}; nevertheless, no distortion of the Pb(111) has been detected in the present experiments. This differs from the adsorption of C_{60} on other metal surfaces, however, where substrate reconstructions have been observed.[15,38,39]

There are two types of analysis in the following subsections. In the first, the observed orientations in the LEED patterns are matched to HOC lattices. This is a geometrical analysis without explicit treatment of the underlying interactions, but it provides an interesting perspective on these large

unit cells. In the second, centrally-symmetric C_{60}-C_{60} pair potentials are used to model the energetics of the monolayer solid and its modulation by a spatially periodic substrate potential. It turns out that the lattice orientations that are observed also arise as local energy minima in the Novaco-McTague perturbation theory of orientational epitaxy.

B. Monolayer solid energies

Table I has data for triangular lattices of spherical C_{60} molecules using the C_{60}-C_{60} pair potential of Girifalco[40] and of Pacheco and Ramalho.[41] The Girifalco (G) potential is widely used for C_{60} modeling, but there are indications that its short-range repulsion is too steep,[35] and the Pacheco-Ramalho (PR) potential fits the 3D pressure-volume data better. For comparison, the two-molecule potential energy $V(R)$ has the following properties for the two potentials: For the G model, the minimum energy is −277 meV at a spacing of $R_0 = 10.055$ Å and $V(R) = 0$ at $R = 9.593$ Å. For the PR model, the minimum energy is −267 meV at a spacing of $R_0 = 10.018$ Å and $V(R) = 0$ at $R = 9.397$ Å.

Most of the spacings treated here for the triangular lattice are in the range $L_{nn} = 9.8 - 10.0$ Å. We infer from Ref. 35 that the use of the spherically averaged pair potential does not introduce serious errors in this range. The 10 Å is set by the spacing in the 3D fcc solid at 300 K and zero pressure. The 9.8 Å is set by an estimated limit of compression for the monolayer. Although the monolayer heat of condensation of C_{60}/Pb(111) is not known, the calculated minimum lateral energy of about −0.8 eV and the 3D heat of sublimation of 1.7 eV suggest that the limit of compression is achieved when the stress term in the enthalpy, the product of the spreading pressure and area per molecule A, is about 1 eV. This occurs for $L_{nn} \approx 9.8$ Å [9.7 Å] for the G [PR] models. The PR model bulk modulus $B = 13.8$ J m^{-2} is already large,

TABLE II. C$_{60}$-C$_{60}$ nearest-neighbor distances on close-packed surfaces.

Substrate	Temperature (K)	Structure	C$_{60}$-C$_{60}$ distance (Å)	Reference
Graphite	50	Incommensurate	9.99 ± 0.01	[43]
Cu(111)	300	4×4 (reconstructed)	10.2	[38]
Al(111)	300	6×6 (buckled)	9.92	[16]
Ag(111)	300	$(2\sqrt{3} \times 2\sqrt{3})R30°$	10.0	[4]
Au(111)	300	$(2\sqrt{3} \times 2\sqrt{3})R30°$	9.99	[4]
Au(111)	5	HOC	10.02	[17]
Pt(111)	300	$(\sqrt{13} \times \sqrt{13})R13.9°$	9.99	[15]
Pb(111)	80	HOC	10.0 ± 0.1	this work

(compressibility is small, 0.07 m^2 J^{-1}, 10–20 times smaller than for Xe on metals[42]) for the compressed lattice at 9.9 Å; this is in accord with the observation that the adlayer modulations in the Moiré patterns are smooth and domain wall structures are broad for C$_{60}$/Pb(111). Table I gives the spreading pressure, energy per particle, and bulk modulus for the two models.

On the basis of these calculations, the anticipated lattice constant of the C$_{60}$ at monolayer condensation is 10.0–10.05 Å and the lattice constant of a monolayer prepared by dosing beyond the monolayer condensation and before further condensation might be as small as 9.7–9.8 Å. The experiment finds an L_{nn} of 10.0 ± 0.1 Å over a range of submonolayer coverages. This constant value may be a result of the overlayer locking into particular HOC structures, as described in the next section. It lies in the narrow range of L_{nn}'s observed for C$_{60}$ on other close-packed metal surfaces and on graphite,[43] as shown in Table II.

C. HOC analysis of the Moiré structures

In order to identify possible HOC structures, we have employed a systematic approach called the "hexagonal number sequence" method proposed by Tkatchenko,[24] as follows. The lattice vectors for the Pb(111) substrate surface are represented by $\mathbf{a_1} = (1,0)a$ and $\mathbf{a_2} = (1/2, \sqrt{3}/2)a$, where a is the nearest-neighbor distance of the Pb atoms. Any lattice point of the substrate can be described as a linear combination of these primitive vectors, $\mathbf{R} = m\mathbf{a_1} + n\mathbf{a_2}$, where m and n are integers. For any commensurate or HOC layer on this substrate, the lattice vectors of the overlayer can be described by the lattice vectors

$$\mathbf{A_1} \quad \text{and} \quad \mathbf{A_2} = \begin{pmatrix} \frac{1}{2} & -\frac{\sqrt{3}}{2} \\ \frac{\sqrt{3}}{2} & \frac{1}{2} \end{pmatrix} \mathbf{A_1},$$

where $\mathbf{A_1}$ and $\mathbf{A_2}$ satisfy $m_0\mathbf{A_1} + n_0\mathbf{A_2} = m\mathbf{a_1} + n\mathbf{a_2}$, where m, n, m_0 and n_0 are integers. The total number of atoms (or molecules) in either the substrate or the overlayer can be expressed with the same mathematical form, $N = m^2 + n^2 + mn$, or $N_0 = m_0^2 + n_0^2 + m_0 n_0$ for the substrate and adsorbate, respectively. Each combination of m, n, m_0, n_0 represents a different commensurate structure of the system and possesses a different relative lattice constant and a different rotation angle. By listing all possible m, n, m_0, n_0 combinations, it is possible to identify which structures have the measured characteristics.

With no other constraints, this method will produce an infinite number of HOCs that will fit the experimental diffraction parameters, because any combination of parameters can be generated using a large enough HOC unit cell. In reality, the size of the HOC unit cell is limited in an experiment by the perfection of the crystal. In this study, we are able to utilize the constraint of the period of the Moiré patterns observed in the STM images.

Table III shows the HOC structure parameters that provide the closest matches to the parameters determined from the LEED and STM experiments. The values of lattice parameter ratio R and lattice angle θ that are consistent with the LEED and STM experiments are indicated by bold type. Only two structures satisfy all of the measured parameters, namely those which correspond to m=2, n=12 and m=9, n=14. These are the HOC structures $(\sqrt{172} \times \sqrt{172})R7.59°$ and $(\sqrt{403} \times \sqrt{403})R22.85°$, respectively, and they have 21 and 49 C$_{60}$ molecules per unit cell, and 172 and 403 Pb atoms per unit cell, respectively. Diagrams of these structures are shown in Fig. 6. The parameters that describe these structures are given in Table IV. Assuming a substrate nearest-neighbor distance (at 80 K) of 3.48 Å, the unit cell sizes for these structures are 45.6 Å and 69.9 Å, with Moiré lengths 45.6 Å and 34.9 Å, respectively.

From the previous derivation used to describe the HOC structures, expressions for the angles of the HOC unit cell to both the substrate lattice and the overlayer lattice can be derived:

$$\theta_{n,m} = \tan^{-1}\left(\frac{\sqrt{3}n}{n+2m}\right); \quad \theta_{n_0,m_0} = \tan^{-1}\left(\frac{\sqrt{3}n_0}{n_0+2m_0}\right),$$

where θ_{nm} and $\theta_{n_0 m_0}$ are the angles between the unit cell and the substrate and overlayer, respectively. The angle θ between the substrate and overlayer lattices is the difference of these angles. The ratio between the overlayer lattice constant and the substrate lattice constant is

$$R = \sqrt{\frac{n^2 + m^2 + nm}{n_0^2 + m_0^2 + n_0 m_0}}.$$

Figure 7 shows θ vs R for any combination of n, m, n_0 and m_0 up to a limiting unit cell size of 70 Å. Each dot in the

TABLE III. HOC structures generated using the experimentally-determined parameters for lattice ratio and lattice rotation angle that have a Moiré size consistent with the STM images. The bold numbers correspond to the values within the experimental error of the LEED experiment. The boxes indicate the HOCs that meet all experimental constraints. This table contains only those structures in the vicinity of the best match.

Structures near the 35 Å Moiré						
m	8	8	8	8	8	8	8
n	11	12	13	14	15	16	17
1/R	0.424	0.401	0.381	0.363	**0.346**	0.331	0.317
θ	24.79	23.41	**22.17**	21.05	20.03	19.11	18.26
m	9	9	9	9	9	9	9
n	11	12	13	14	15	16	17
1/R	0.403	0.384	0.365	**0.349**	0.333	0.319	0.306
θ	26.70	25.28	24.01	**22.85**	**21.79**	20.85	19.93
m	10	10	10	10	10	10	10
n	11	12	13	14	15	16	17
1/R	0.385	0.367	**0.350**	0.335	0.321	0.308	0.296
θ	28.43	27.00	25.69	24.50	23.41	**22.41**	21.49

Structures near the 46 Å Moiré						
m	2	2	2	2	2	2	2
n	9	10	11	12	13	14	15
1/R	0.452	0.412	0.378	**0.349**	0.325	0.303	0.285
θ	20.72	19.84	**19.11**	**18.48**	**17.95**	17.48	17.07

figure represents a different commensurate structure. The primitive commensurate structures appear as points of higher symmetry. The "void" having no points around each primitive structure arises because the HOC's near these structures have large unit cells and are excluded from this graph. It is evident in Fig. 7 that many HOC structures are consistent with the experimental lattice ratio $R = 2.87$. There is no plausible stabilization energy that can be identified in this context to explain why two of these HOC's would be selected. To gain more insight into the lattice rotations, we consider the Novaco-McTague perturbation theory of orientational epitaxy.

D. Novaco-McTague perturbation theory analysis

There are examples in physical adsorption[44] where the orientation of an overlayer lattice is set by energetic considerations for mass density waves within the adsorbed layer, as described by the NM perturbation theory.[18,19] The results of calculations for the present system using the two-dimensional (2D) (no z modulation) version of the original 2nd-order perturbation NM theory[19] are presented in Table V for the two different potential models described earlier. The local NM minimum energy can be determined in the 2D approximation without knowing the value of the corrugation energy amplitude V_g in the molecule-substrate potential energy. There is an overall scale factor V_g^2 in the perturbation energy that would need to be supplied from the C_{60}-Pb in-

teraction in order to obtain numerical energies.

The mass density waves in the lattice are characterized by a misfit wave vector $\mathbf{q_M}$ that includes both the difference in average periods of the film and the substrate and the different alignment of the two lattices. The misfit wave vectors that enter in the adlayer modulation are expected to be based on the leading substrate reciprocal lattice vectors $\mathbf{g_0} = 2.085$ Å^{-1} and multiples of the primitive reciprocal lattice vector of the adlayer $\boldsymbol{\tau_0} = 4\pi/\sqrt{3}L_{nn}$. The values of the misfit wave number q_M for lattices corresponding to 3×3 and $(\sqrt{7} \times \sqrt{7})R19.11°$ superlattices are $q_M(3) = g_0 - 3\tau_0$ and $q_M(\sqrt{7}) = g_0 - \sqrt{7}\tau_0$, respectively. There is a cross-over where their magnitudes are equal to each other, i.e., $|q_M(3)| = |q_M(\sqrt{7})|$, at $L_c = 9.82$ Å. For $L_{nn} > L_c$, $|q_M(3)| < |q_M(\sqrt{7})|$ and vice versa.

Because of the large difference in nearest-neighbor spacings in the Pb substrate and the C_{60} monolayer, misfit wave vectors between the primitive substrate reciprocal lattice vectors and higher reciprocal lattice vectors of the monolayer must be treated. For monolayer lattice constants decreasing from 10 Å, there are additional local energy minima as a function of orientation angle, and for lattice constants near 9.8 Å the new minima become the lowest energy orientations.

Table V reports the angles for the local minimum energies for different L_{nn}'s. The results in the Table for the angles are first expressed relative to 0 degrees, which is the alignment of the 3×3 superlattice ($L_{nn} = 10.44$ Å) and then relative to 19.11°, which is the angle of the $(\sqrt{7} \times \sqrt{7})R19.11°$ superlat-
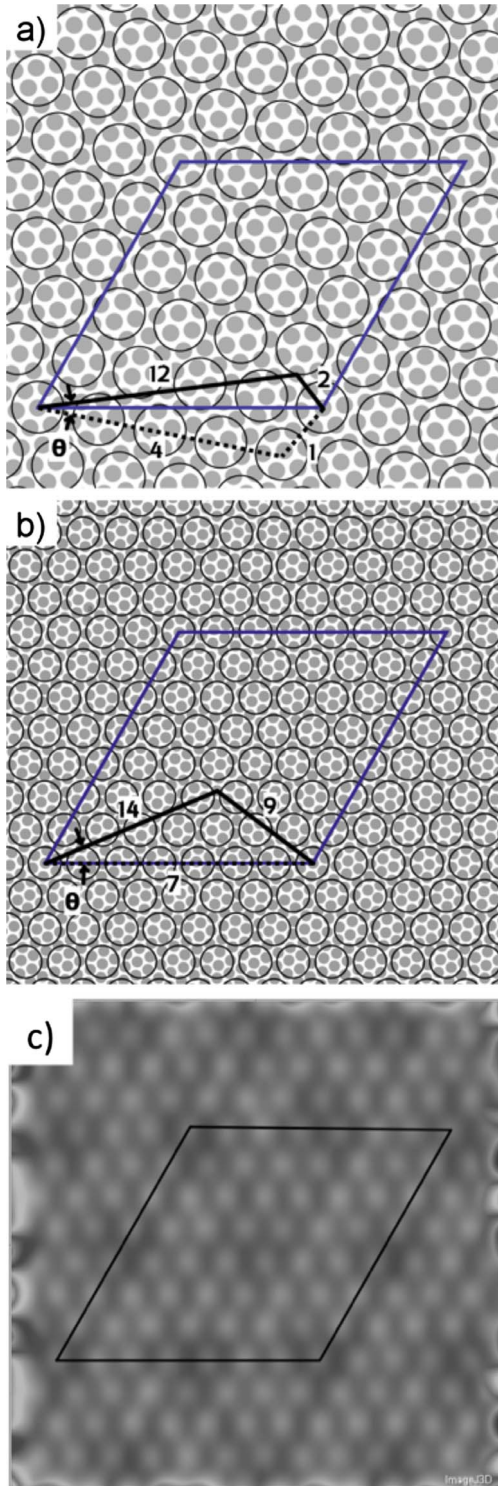
FIG. 6. (Color online) (a) Structure diagram for ($\sqrt{172}$ × $\sqrt{172}$)R7.59°. The rhombus indicates the HOC unit cell, which is the same as the Moiré size for this structure. The numbers indicate the parameters corresponding to the hexagonal number sequence method. The angle θ is the angle of rotation between the substrate and overlayer lattices. (b) Structure diagram for ($\sqrt{403}$ × $\sqrt{403}$)R22.85°. For this structure, the length of the Moiré pattern is half of the unit cell length, as shown in (c). (c) Smoothed intensity map of the structure shown in (b), on the same scale, showing that the apparent Moiré structure has half the period of the HOC.

tice (L_{nn}=9.21 Å). These two superlattices are the nearest candidates with only one C$_{60}$ in the unit cell, and they have 9 and 7 Pb atoms per (3×3) or $\sqrt{7}$ unit cell, respectively. The calculated energies and spreading pressures presented in Table I show that both of these simple superlattices would be under considerable stress, which helps to explain why they do not form on Pb(111).

The angles for L_{nn} in the range 9.95–9.40 Å have the interesting feature that they are nearly symmetric pairs about the $\sqrt{7}$ alignment of 19.11°. These become the minimum energy alignment at L_{nn} in the range where the smaller magnitude misfit wave vector is $|q_M(\sqrt{7})|$, i.e., for $L_{nn} < 9.82$ Å. The misfit wave vector q_M for the leading substrate reciprocal lattice vector g$_0$ seems to automatically be taken relative to the $\sqrt{7}\tau_0$ reciprocal lattice vector of the adlayer as the alignment angle is varied in the perturbation theory. The splitting of the C$_{60}$ LEED spots in Fig. 1 is about 4°, which is close to the calculated splitting at L_{nn}=9.8 Å.

IV. DISCUSSION AND CONCLUSION

The experimental results for the incommensurate monolayer of C$_{60}$ on Pb(111) show the presence of two differently oriented overlayer structures, having angles of 18.6 ± 0.7 and 22.4 ± 0.7 degrees relative to the Pb symmetry direction, and having the same or nearly the same lattice constant, 10.0 ± 0.1 Å. We have presented an analysis that indicates that these may be identified as particular HOC structures. Finally, we have applied an NM analysis to this monolayer, which indicates solutions having similar epitaxial angles to those observed. Although the numerical agreement between the experiment and the calculated NM angles is remarkable considering all of the possible pitfalls (see below), there is a small discrepancy concerning the lattice constant at which these angles are observed. In the experiment, the lattice constant was measured to be 10.0 ± 0.1 Å, but the theory finds similar angles to be energetically preferred only for lattice constants of 9.82 Å or less. We note, however, that the thermodynamic interpretation of the observed orientations is
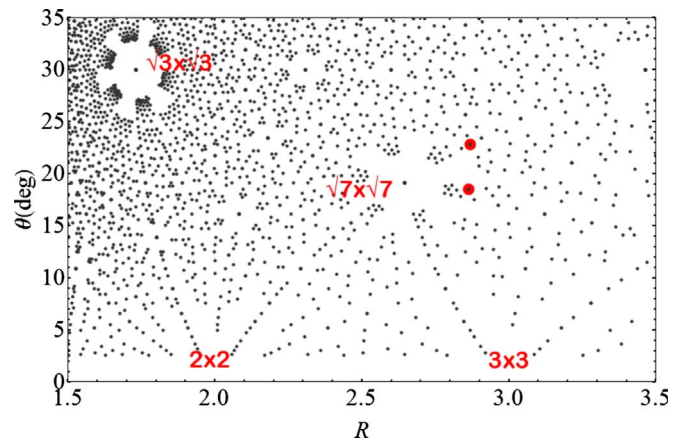

FIG. 7. (Color online) All HOC structures having unit cells up to 70 Å, indicated as small dots. The HOC structures found to agree best with the experimental data are indicated as larger (red) dots.

TABLE IV. Parameters for the two best-fit HOC structures.

Parameter	$(\sqrt{403} \times \sqrt{403})R22.85°$	$(\sqrt{172} \times \sqrt{172})R7.59°$	LEED/STM
Lattice ratio 1/R	0.349	0.349	0.348 ± 0.004
C_{60}-C_{60} distance	9.96 Å	9.96 Å	10.0 ± 0.1 Å
Rotation angle between C_{60} rows and Pb rows	22.85°	18.48°	$22.4 \pm 0.7°$, $18.6 \pm 0.7°$
m	9	2	
n	14	12	
m_0	7	1	7, 1
n_0	0	4	0, 4
N	403	172	
N_0	49	21	
Transfer matrix	$\begin{pmatrix} 9 & -14 \\ 14 & 23 \end{pmatrix}$	$\begin{pmatrix} 2 & -12 \\ 12 & 14 \end{pmatrix}$	

simpler for the NM theory than for the HOC identification. In the NM theory, the two orientations arise from equivalent domains of the monolayer solid, while the assignment of the two orientations to different HOC structures requires a metastable coexistence of two distinct solid phases. The difference in their thermodynamic potentials may be small enough that this does not become a serious quantitative problem, but it is a conceptual one, and even more confusing when considering the additional orientations evident in Fig. 7.

There are a few problems that might be expected in the application of the NM theory to this case. First, the theory assumes that the substrate is rigid. No reconstruction or deformation of the substrate was detected in these experiments, but neither STM nor LEED would be sensitive to small deformations in the substrate, which seem likely to occur based on the low substrate:overlayer ratio of bulk moduli in this case. Second, this application of the theory ignores any z modulation of the structure, which is likely to be present based on the modulation observed in the tunneling spectroscopy. Third, the C_{60}-C_{60} potential might differ from the assumed forms. The most likely deviation is a dipole repulsion

term that would result from the charge transfer between the C_{60} and the substrate, but the nature of the bonding between the C_{60} molecules and the Pb(111) is not yet known, although our tunneling spectroscopy experiments indicate a small LUMO tail extending across the Fermi level, implying some charge transfer. This brings up an important point, that we are using modeling that is normally applied to physisorption systems to describe a system that may have chemical interactions. However, we note that the NM theory is not restricted to physisorption and has been applied to chemisorption systems such as alkali metals on metals.[45] The level of agreement found in the present case suggests, however, that the C_{60}-Pb potential energy is weakly corrugated, which might also imply a relatively weak C_{60}-Pb interaction compared to other metals, where significant substrate reconstructions are apparent.[15,16,38,46]

There are other geometrical models for orientational epitaxy that we have not considered here, including the Bohr-Grey model[23] that treats the alignment of the modulation wave vector with the substrate or overlayer symmetry directions. This model predicts possible trajectories of the epitax-

TABLE V. Orientational epitaxy angles (in degrees) relative to 0° and the 19.11° alignment of the $(\sqrt{7} \times \sqrt{7})R19.1°$ structure, for C_{60}/Pb(111) with the G and P-R potential models and NM perturbation theory. The angles near 0° are energetically preferred (shown in bold) for $L_{nn} > 9.82$ Å, whereas the angles near 19° are preferred (shown in bold) for smaller L_{nn}.

L_{nn} (Å)	Girifalco		Pacheco-Ramalho	
	θ (° relative to 0)	θ (° relative to $\sqrt{7}$)	θ (° relative to 0)	θ (° relative to $\sqrt{7}$)
10.45	<0.001		0.0134	
L_u	**1.36**, 16.56, 22.43	−2.55, +3.32	**1.53**, 16.82, 22.24	−2.29, +3.13
9.95	**1.83**, 16.89, 22.01	−2.22, +2.90	**1.82**, 16.90, 22.00	−2.21, +2.89
9.90	**2.09**, 16.98, 21.80	−2.13, +2.69	**2.09**, 16.98, 21.80	−2.13, +2.69
9.85	**2.38**, 17.08, 21.59	−2.03, +2.48	**2.39**, 17.08, 21.59	−2.03, +2.48
9.8	2.72, **17.19, 21.39**	−1.92, +2.28	2.73, **17.18, 21.39**	−1.93, +2.28
9.75	3.22, **17.31, 21.18**	−1.80, +2.07	3.15, **17.30, 21.20**	−1.81, +2.09
9.4	**18.40, 19.83**	−0.71, +0.72	**18.38, 19.85**	−0.73, +0.74

ial angle as a function of the lattice misfit, but is not based on quantitative balancing of adatom-adatom and adatom-substrate interaction terms, and also it does not predict discrete structures.

To summarize, our experiments have found two coexisting close-packed structures for a C$_{60}$ monolayer on Pb(111). These structures have nonsymmetrical epitaxial orientations, and we have identified two higher-order commensurate structures that are consistent with the observations. The Novaco-McTague analysis for this layer finds two similarly rotated structures for lattice constants about 0.2 Å smaller than that found in the experiments. This level of agreement suggests that this adsorption system represents a case of a weakly interacting adsorption system, unlike the situation for C$_{60}$ on other metal surfaces.[16] The tunneling spectroscopy of the fullerenes across the Moiré structure indicates that the energetic alignment of the molecular resonances is modulated with the Moiré pattern, also consistent with small variations in the substrate potential across the Moiré unit cell.

[1] E. Osawa, *Perspectives in Fullerene Nanotechnology* (Kluwer Academic Publishers, Dordrecht, 2002).

[2] M. C. Petty, *Molecular Electronics: From Principles to Practice* (John Wiley and Sons, Chichester, 2007).

[3] S. M. Gatica, M. M. Calbi, R. D. Diehl, and M. W. Cole, J. Low Temp. Phys. **152**, 89 (2008).

[4] E. I. Altman and R. J. Colton, Phys. Rev. B **48**, 18244 (1993).

[5] A. Fartash, Phys. Rev. B **52**, 7883 (1995).

[6] T. Hashizume and T. Sakurai, Surf. Rev. Lett. **3**, 905 (1996).

[7] T. Sakurai, X. D. Wang, T. Hashizume, V. Yurov, H. Shinohara, and H. W. Pickering, Appl. Surf. Sci. **87-88**, 405 (1995).

[8] L. L. Wang and H. P. Cheng, Phys. Rev. B **69**, 165417 (2004).

[9] X. D. Wang, S. Yamazaki, J. L. Li, T. Hashizume, H. Shinohara, and T. Sakurai, Scanning Microsc. **8**, 987 (1994).

[10] E. I. Altman and R. J. Colton, J. Vac. Sci. Technol. B **12**, 1906 (1994).

[11] J. K. Gimzewski, S. Modesti, T. David, and R. R. Schlittler, J. Vac. Sci. Technol. B **12**, 1942 (1994).

[12] C. Rogero, J. I. Pascual, J. Gomez-Herrero, and A. M. Baro, J. Chem. Phys. **116**, 832 (2002).

[13] T. Hashizume, K. Motai, X. D. Wang, H. Shinohara, H. W. Pickering, and T. Sakurai, J. Vac. Sci. Technol. A **12**, 2097 (1994).

[14] T. Hashizume, K. Motai, X. D. Wang, H. Shinohara, and T. Sakurai, Science Reports of the Research Institutes Tohoku University Series A: Physics Chemistry and Metallurgy **39**, 51 (1993).

[15] R. Felici, M. Pedio, F. Borgatti, S. Iannotta, M. Capozi, G. Ciullo, and A. Stierle, Nature Mater. **4**, 688 (2005).

[16] A. J. Maxwell, P. A. Brühwiler, D. Arvanitis, J. Hasselström, M. K.-J. Johansson, and N. Mårtensson, Phys. Rev. B **57**, 7312 (1998).

[17] G. Schull and R. Berndt, Phys. Rev. Lett. **99**, 226105 (2007).

[18] J. P. McTague and A. D. Novaco, Phys. Rev. B **19**, 5299 (1979).

[19] A. D. Novaco and J. P. McTague, Phys. Rev. Lett. **38**, 1286 (1977).

[20] L. W. Bruch, in *Phase Transitions in Surface Films 2*, edited by H. Taub, G. Torzo, H. J. Lauter, and S. C. Fain (Plenum, New York, 1991), p. 67.

[21] G. S. Leatherman, R. D. Diehl, M. Karimi, and G. Vidali, Phys. Rev. B **56**, 6970 (1997).

[22] C. G. Shaw, S. C. Fain, Jr., and M. D. Chinn, Phys. Rev. Lett. **41**, 955 (1978).

[23] F. Grey and J. Bohr, in *Phase Transitions in Surface Films 2*, edited by H. Taub, G. Torzo, H. J. Lauter, and S. C. Fain, Jr. (Plenum Press, New York, 1991), p. 83.

[24] A. Tkatchenko, Phys. Rev. B **75**, 235411 (2007).

[25] P. Bak, Rep. Prog. Phys. **45**, 587 (1982).

[26] N. Ferralis, H. I. Li, K. J. Hanna, J. Stevens, H. Shin, F. M. Pan, and R. D. Diehl, J. Phys.: Condens. Matter **19**, 056011 (2007).

[27] G. Schulze, K. J. Franke, and J. I. Pascual, New J. Phys. **10**, 065005 (2008).

[28] C. Silien, N. A. Pradhan, W. Ho, and P. A. Thiry, Phys. Rev. B **69**, 115434 (2004).

[29] X. Lu, M. Grobis, K. H. Khoo, S. G. Louie, and M. F. Crommie, Phys. Rev. B **70**, 115418 (2004).

[30] I. Fernandez-Torrente, K. J. Franke, and J. I. Pascual, J. Phys.: Condens. Matter **20**, 184001 (2008).

[31] K. J. Franke, G. Schulze, N. Henningsen, J. I. Pascual, S. Zarwell, K. Rück-Braun, M. Cobian, and N. Lorente, Phys. Rev. Lett. **100**, 036807 (2008).

[32] P. A. Heiney, J. E. Fischer, A. R. McGhie, W. J. Romanow, A. M. Denenstein, J. P. McCauley, A. B. Smith, and D. E. Cox, Phys. Rev. Lett. **66**, 2911 (1991).

[33] J. E. Fischer, P. A. Heiney, A. R. McGhie, W. J. Romanow, A. M. Denenstein, J. P. McCauley, and A. B. Smith, Science **252**, 1288 (1991).

[34] C. Pan, M. P. Sampson, Y. Chai, R. H. Hauge, and J. L. Margrave, J. Phys. Chem. **95**, 2944 (1991).

[35] M. C. Abramo, C. Caccamo, D. Costa, G. Pellicane, and R. Roberto, Phys. Rev. E **69**, 031112 (2004).

[36] G. Simmons and H. Wang, in *Single Crystal Elastic Constants and Calculated Aggregate Properites: A Handbook*, 2nd edition (MIT Press, Cambridge, MA, 1971).

[37] P. Korpiun, W. Albrecht, T. Muller, and E. Lüscher, Phys. Lett. A **48**, 253 (1974).

[38] W. W. Pai, C. L. Hsu, M. C. Lin, K. C. Lin, and T. B. Tang, Phys. Rev. B **69**, 125405 (2004).

[39] X. Zhang, W. He, A. Zhao, H. Li, L. Chen, W. W. Pai, J. Hou, M. M. T. Loy, J. Yang, and X. Xiao, Phys. Rev. B **75**, 235444 (2007).

[40] L. A. Girifalco, J. Phys. Chem. **96**, 858 (1992).

[41] J. M. Pacheco and J. P. P. Ramalho, Phys. Rev. Lett. **79**, 3873 (1997).

[42] L. W. Bruch, R. D. Diehl, and J. A. Venables, Rev. Mod. Phys. **79**, 1381 (2007).

[43] H. Shin and R. D. Diehl (unpublished).

[44] L. W. Bruch, M. W. Cole, and E. Zaremba, *Physical Adsorption: Forces and Phenomena* (Dover, New York, 2007).

[45] G. S. Leatherman and R. D. Diehl, Phys. Rev. B **53**, 4939 (1996).

[46] M. K.-J. Johansson, A. J. Maxwell, S. M. Gray, P. A. Brühwiler, and L. S. O. Johansson, Surf. Sci. **397**, 314 (1998).